Simultaneous Prediction of Crystal Shape and Size for Solution Crystallization

Yongchun Zhang and Michael F. Doherty
Dept. of Chemical Engineering, University of California, Santa Barbara, CA 93106

DOI 10.1002/aic.10182
Published online in Wiley InterScience (www.interscience.wiley.com).

Crystals experience changes in both size and shape during growth. A method is developed for the simultaneous prediction of crystal shape evolution and size distribution for solution crystallization processes by combining shape evolution modeling and population balance modeling techniques. When surface integration is the rate-controlling step and each face grows by the same mechanism (for example, the screw dislocation mechanism), the relative growth rates of crystal faces are constant, and the crystal volume can be represented by a piecewise smooth function of the crystal size. The process can then be described by a simple 1-dimensional (1-D) population balance model linked with the shape evolution model. The current method is applicable to tablet-shaped crystals with a dominant face of arbitrary initial size and shape. Such crystals can be treated as two-dimensional (2-D). A case study of succinic acid crystals grown from water illustrates the applicability and simplicity of the proposed method. © 2004 American Institute of Chemical Engineers *AIChE J,* 50: 2101–2112, 2004
Keywords: crystallization, shape evolution, population balance, shape factor, succinic acid

Introduction

Crystals produced by solution crystallization have distinct morphologies and a distribution of sizes. The shape and size of crystals are two important factors for product quality, as well as the design and operation of solid-liquid separation systems. Continuous crystallizers operate at low-supersaturation (slow growth) and finite residence times, with the result that most crystals in the crystallizer are not in their steady-state shape. Moreover, the shape of a crystal changes along with its size during growth. Researchers have extensively studied the morphology of crystals, as well as the population balance dynamics for the crystal-size distribution (CSD) in different types of crystallizers. However, very little attention has been given to the simultaneous prediction of crystal shape and size distribution.

Gadewar and Doherty (2004) recently developed a methodology that allows for the prediction of the shape evolution of 2-D crystals from arbitrary initial shapes. Based on this method, by making further assumptions that: (a) all growing crystal faces follow the same growth mechanism (for example, screw-dislocation mechanism) having the same dependence on supersaturation, and (b) the relative face growth rates are constant and predictable, we conclude that crystals with a known initial size and shape will follow fixed shape evolution "trajectories" during their growth. Consequently, if all the crystals are assumed to grow from nuclei with identical size and shape, the crystal shape may be simply characterized by a shape factor which can be predicted from the shape evolution model, and depends only on the instantaneous crystal size. This observation enables the simultaneous prediction of crystal shape evolution and size distribution by combining shape evolution and population balance modeling. The objective of this research, therefore, is to link population balance models with the shape evolution model to provide a novel method for simultaneously predicting the crystal shape evolution and size distribution.

The rest of this article is organized as follows: first, the crystal shape evolution model for 2-D crystals is briefly re-

Correspondence should be addressed to M. F. Doherty at mfd@engineering.ucsb.edu.

viewed and some of its applications are studied; the population balance model for an ideal mixed suspension mixed product removal (MSMPR) crystallizer which accounts for the shape evolution of crystals is then presented, and its numerical solution methods are discussed, followed by a case study for succinic acid crystals grown from water and discussion on some practical issues.

Crystal Shape Evolution

The shape, or habit, of a crystal is determined by all the crystallographic faces and their relative normal distances from an origin inside the crystal. Crystals can have very different habits, for example, cubic, plate, needle, fiber-like, and so on (Randolph and Larson, 1988). The steady-state habit of some crystals can be predicted by studying their solid-state molecular structure and the solvent effects (Liu et al., 1995; Winn and Doherty, 1998; Bisker-Leib and Doherty, 2003). Of particular interest to us are the crystals which grow into plate-like habits, such as succinic acid grown from water (Mullin and Whiting, 1980; Winn and Doherty, 1998), vanillin grown from chloroform (Singh et al., 1991), and biphenyl grown from toluene (Jetten et al., 1984). Since crystals with such a habit have one dominant face, they can be viewed as 2-D by projection onto the dominant face.

The shape of crystal seeds obtained by mechanical grinding or born from nucleation, attrition or breakage are normally very different from the steady-state habit. However, a crystal will eventually grow into its steady-state shape provided that it is exposed to a supersaturated solution for sufficient time. A crystal can have many faces that grow at different velocities and faces may appear and disappear during the growth due to the difference in growth rates (Szurgot and Prywer, 1991; Prywer, 1996; Gadewar and Doherty, 2004). Therefore, it is possible to predict the evolution of crystal shape if the face growth rates are known.

Growth velocities

The commonly used crystal face growth rates reported in the literature refer to the velocity of a crystal face in the normal direction. Crystal faces grow by different kinetic mechanisms. Under high supersaturation (over 50%), crystals can grow by either the rough growth or the surface nucleation mechanisms; for crystallization process under low supersaturation, crystals grow by the screw-dislocation mechanism, also known as spiral growth, BCF growth, and so on (Burton et al., 1951). Since we are primarily interested in continuous crystallizers with low supersaturation, it is reasonable to assume that all crystal faces follow the BCF growth mechanism.

Winn and Doherty (1998, 2000) point out that for solution crystallization with surface integration-controlled growth, the relative growth velocity of a crystal face is dependent only on the kink free energy, which represents the likeliness of new solute molecules attaching to a given face. The kink free energies can be calculated, and are independent of either crystal size or supersaturation, that is, the kink free energy of each face is fixed for a given pair of solute and solvent. The crystal growth rate for face i can be written as

$$G_i = f(\phi_i^{\text{kink}})\, g(\sigma)$$

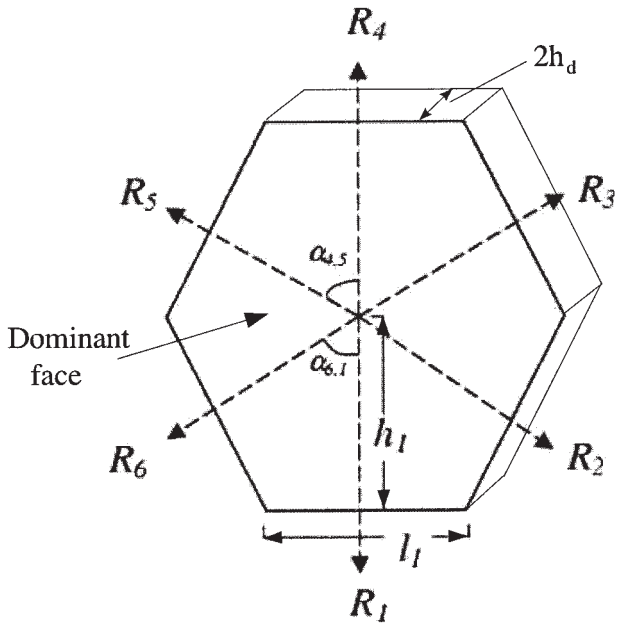

Figure 1. 2-D crystal.

where ϕ_i^{kink} stands for the kink free energy of face i, and $\sigma = (c - c_s)/c_s$ is the relative supersaturation. The ratio of growth rates between two faces is constant, independent of the supersaturation

$$R_{ij} = \frac{G_i}{G_j} = \frac{f(\phi_i^{\text{kink}})}{f(\phi_j^{\text{kink}})}$$

Therefore, under these growth conditions, crystals grown from a given solvent will have a fixed shape at a given size if the initial seed or nucleus shape and size are predetermined. This is equivalent to saying that all crystals evolving from the seeds with a certain size and shape will follow the same "shape evolution trajectory." Consequently, this enables the linking of the crystal shape evolution (CSE) model to the population balance model (PBM) by a volume shape factor k_v, depending only on the crystal size. This conclusion will be further illustrated later in the article.

Meanwhile, crystal faces also experience tangential expansion or shrinkage during growth, due to the difference in growth velocities of the adjacent faces. For a 2-D crystal, the tangential growth rate of a given face can be calculated using Kozlovskii's model (1957), using the perpendicular growth velocities of faces G_i, and the angles between the faces $\alpha_{i,j}$

$$v_i = \frac{dl_i}{dt} = \frac{G_{i+1} - G_i \cos\alpha_{i,i+1}}{\sin\alpha_{i,i+1}} + \frac{G_{i-1} - G_i \cos\alpha_{i-1,i}}{\sin\alpha_{i-1,i}} \quad (1)$$

where v_i is the tangential growth velocity and l_i is the length of face i (see Figure 1).

Shape evolution model

In this section we summarize the shape evolution model of Gadewar and Doherty (2004) and introduce the dimensionless variables used in the model formulation and solution.

Assume we can identify a reference face (hkl) that will never disappear during the growth and its absolute growth rate is known to be $G_{hkl} = f(\phi_{hkl}^{\text{kink}})\, g(\sigma)$. The relative growth rates

$$R_i = \frac{G_i}{G_{hkl}}$$

are then constant and can be calculated using first principles method such as Winn and Doherty (1998) and Liu et al. (1995).

Using the relative growth rates, Eq. 1 can be rewritten as

$$v_i = \frac{dl_i}{dt} = G_{hkl}\left(\frac{R_{i+1} - R_i \cos\alpha_{i,i+1}}{\sin\alpha_{i,i+1}} + \frac{R_{i-1} - R_i \cos\alpha_{i-1,i}}{\sin\alpha_{i-1,i}}\right) \tag{2}$$

It is worth noticing that v_i may be negative, which indicates the possibility that the corresponding face may disappear during crystal growth.

Define a new variable $y_i = v_i/G_{hkl}$. We can write a dimensionless tangential growth model as

$$y_i = \frac{v_i}{G_{hkl}} = \frac{R_{i+1} - R_i \cos\alpha_{i,i+1}}{\sin\alpha_{i,i+1}} + \frac{R_{i-1} - R_i \cos\alpha_{i-1,i}}{\sin\alpha_{i-1,i}} \tag{3}$$

Since R_i and $\alpha_{i,j}$ are constant, y_i is also constant. Following the method of Gadewar and Doherty (2004), we can derive the CSE model as follows

$$\frac{dx_i}{d\xi} = u_i - x_i \tag{4}$$

$$\frac{dL}{d\xi} = L \tag{5}$$

Where $L = \Sigma_i\, l_i$ is the perimeter of the crystal, $V = \Sigma_i\, v_i$ is the summed tangential growth rates, $x_i = l_i/L$ and $u_i = (v_i/V)$ are the dimensionless length and tangential growth rate for face i, respectively; the value of each u_i is constant. The dimensionless warped time ξ is defined as $d\xi = (V/L)dt$.

Defining $\xi = 0$ at $t = 0$, solving the above equations yields

$$L = L^0 + \int_0^t V dt = L^0 \exp(\xi) \tag{6}$$

$$x_i = u_i - (u_i - x_i^0)\exp(-\xi) = u_i - (u_i - x_i^0)\frac{L^0}{L} \tag{7}$$

where L^0 and x_i^0 stand for the initial perimeter and relative length, respectively. From Eq. 6, the dimensionless time $\xi = \ln(L/L^0)$ represents the increase in crystal size relative to its initial size. It is important to note that the physical requirement $x_i \geq 0$ must be imposed on the CSE model. When $u_i \geq 0$ for all faces, $x_i(\xi)$ will converge asymptotically to the steady-state solution $x_i = u_i$ for every face. Faces with negative tangential growth rates may disappear during the growth and never appear again. When a face disappears, the CSE model is revised with the corresponding faces removed. The new initial condition is set to the transition moment, and the parameters $\alpha_{i,j}$, v_i, and u_i are recalculated. The new values of $\alpha_{i,j}$ and u_i are also constant and the remaining x_i's still depend only on the crystal size. Therefore, the crystal shape is determined by the crystal size, as stated previously.

Shape factors

From the CSE model, we can obtain the normal distance h_i of face i from the crystal center (see Figure 1) as

$$h_i = h_i^0 + \int_0^t G_i dt = h_i^0 + \frac{R_i}{Y}(L - L^0) \tag{8}$$

where h_i^0 is the initial distance, $Y = \Sigma_i\, y_i = V/G_{hkl}$ is a constant for any growth period during which no faces disappear. New faces may appear (with $l_i = 0$ and $h_i \neq 0$) at time zero, or at later times.

The area of the dominant face of a 2-D crystal, A_{cryst} can then be calculated as follows by the method of triangulation

$$A_{\text{cryst}} = \frac{1}{2}\sum_{i=1}^{M} l_i h_i \tag{9}$$

Where M stands for the total number of edges on the dominant face. A shape factor k_a can then be defined to relate this area to the characteristic length h_{hkl}

$$k_a(h_{hkl}) = \frac{A_{\text{cryst}}}{h_{hkl}^2}$$

This shape factor is a continuous and piecewise smooth function of h_{hkl}, see Appendix B for proof.

The crystal population balance and solute mass balance require that the volume of crystals be calculated. Recognizing that the dominant face is also normally growing at a fixed growth rate, R_d, relative to the reference face, the normal distance of this dominant face h_d (see Figure 1), can be calculated in the same way as Eq. 8

$$h_d = h_d^0 + \int_0^t G_d dt = h_i^0 + \frac{R_d}{Y}(L - L^0)$$

The volume of crystal is then

$$V_{\text{cryst}} = 2h_d \cdot A_{\text{cryst}}$$

A volumetric shape factor can be defined as

$$k_v(h_{hkl}) = \frac{V_{\text{cryst}}}{h_{hkl}^3} = \sum_i [\alpha_i + \beta_i(h_{hkl} - h_{hkl}^0)^{-1} + \gamma_i(h_{hkl} - h_{hkl}^0)^{-2} + \zeta_i(h_{hkl} - h_{hkl}^0)^{-3}] \tag{10}$$

where the coefficients are defined as

$$\alpha_i = u_i R_i R_d Y, \quad \beta_i = (u_i h_i^0 Y + R_i x_i^0 L^0) R_d + u_i R_i h_d^0 Y$$

$$\gamma_i = x_i^0 h_i^0 L^0 R_d + (u_i h_i^0 Y + R_i x_i^0 L^0) h_d^0, \quad \zeta_i = x_i^0 h_i^0 L^0 h_d^0$$

Like the area shape factor, this volumetric shape factor is also a continuous and piecewise smooth function of h_{hkl}. From Eq. 10, it is clear that the volume shape factor of a crystal depends only on the current crystal size and its initial size and shape. The volume of crystals of any size in the crystallizer can then be easily calculated. By using one characteristic crystal size and the shape factor to identify both the size and shape of a crystal, we are able to capture all of the crystal dimensions without the need to formulate complex and computationally expensive multiple dimensional PBMs for the CSD dynamic simulation.

Population Balance Model

Since its first introduction into chemical engineering (Hulburt and Katz, 1964), population balance modeling has become the standard method for studying the size distribution for particulate systems such as crystallization, polymerization, and biochemical reactors. The classic book by Randolph and Larson (1988) has extensively covered the population balance modeling of crystallization processes.

Theoretically, a multidimensional population balance model can be used to describe the crystal growth in all major crystallographic dimensions, and, therefore, to capture the CSD and crystal shape evolution, simultaneously (Randolph and Larson, 1988). However, the lack of detailed knowledge about crystal face growth kinetics, and the computational challenge limited the practical application of multidimensional PBMs. As a result, most researchers choose to use 1-D PBMs to model crystallization processes. The common approach is to use one characteristic length to identify a crystal, and use a fixed shape factor for all crystals for the mass balance modeling. Others have used crystal volume or mass as the internal coordinate. The disadvantage is that these methods fail to acknowledge the difference in crystal shapes, not to mention the shape evolution during growth. Recently, some researchers (Ma et al., 2002) have successfully used advanced numerical simulation methods for multidimensional PBM for simultaneous CSD and crystal shape prediction. These models typically capture 2 internal dimensions. In reality, there are many internal dimensions that define the crystal shape, but a practical multidimensional PBM still can only capture crystal growth in a limited number of directions, and therefore, is not able to fully track crystal shape evolution. However, as discussed in the Crystal Shape Evolution section, the different characteristic dimensions of a crystal do not change completely independently of each other. Instead, they are related by Eq. 1. Therefore, with the knowledge from the CSE model, it is possible to develop a 1-D PBM, which captures all crystal dimensions and predict the shape evolution simultaneously with size evolution.

Continuous crystallizers

In real continuous crystallizers, crystals experience different local conditions, such as temperature and supersaturation, due to lack of perfect mixing. A realistic model intended to accurately account for these effects requires modeling the complex fluid dynamics to determine the flow field and particle trajectories, as well as the temperature and supersaturation fields. This remains a challenging task. As an alternative, researchers (Benallou et al., 1986; Kramer et al., 1996) developed the compartmental modeling technique to achieve comparable results. The whole crystallizer is normally divided into several compartments. Each compartment is modeled as a well-mixed subsystem, with material and energy exchanges between compartments. Bermingham et al. (1998) demonstrated that using 5–10 compartments is normally adequate to model a pilot plant scale crystallizer.

The objective of the current study is to demonstrate how the crystal shape and size distribution evolution modeling techniques can be coupled. Therefore, we only demonstrate our method by application to an idealized system. In principle, our method can be embedded in the compartment modeling framework.

Consider a continuous crystallization process with the following assumptions:

- Constant volume, isothermal MSMPR crystallizer.
- Secondary contact nucleation only, no crystal fusion or fission.
- No crystals in the feed stream.
- Size-independent growth rates (McCabe's law).
- All faces follow the same growth mechanism.
- All nuclei have the same initial size and shape.
- A reference face exists at time zero and never disappears.

Many of these assumptions can be removed without disturbing the basic framework developed here. As mentioned in the previous section, we label a reference face as (hkl), and define the perpendicular distance from the center of the crystal to the reference face h_{hkl} as the characteristic size of the crystal. Denoting the normal growth velocity of the reference face as $G_{hkl} = dh_{hkl}/dt$, we can then write the complete model, accounting for both the crystal population balance and the solute mass balance in the solution as follows

$$\frac{\partial n}{\partial t} = -G_{hkl}\frac{\partial n}{\partial h_{hkl}} - \frac{n}{\tau} \tag{11}$$

$$\frac{dc}{dt} = \frac{(\rho - c)}{\tau} + \frac{(c_{in} - \rho)}{\varepsilon\tau} + \frac{(\rho - c)}{\varepsilon}\frac{\mathrm{d}\varepsilon}{\mathrm{dt}} \tag{12}$$

where $n(h_{hkl}, t)$ is the crystal number density function, expressed as number of crystals per unit size per unit total volume in the crystallizer, τ is the residence time of the crystallizer, $c(t)$ is the solute concentration in the solution, ρ is the mass density of the crystal, c_{in} is the solute concentration in the feed stream, and ϵ stands for the volume fraction of liquid phase in the crystallizer. The auxiliary equations for the growth rate, the boundary and initial conditions, and so on, are

$$\varepsilon(t) = 1 - \int_0^\infty k_v(h_{hkl}) h_{hkl}^3 n(h_{hkl}, t)\, dh_{hkl} \tag{13}$$

$$G_{hkl}(h_{hkl}, t) = f(\phi_{hkl}^{\mathrm{kink}})\, g(c - c_s) \tag{14}$$

$$\text{Boundary Condition:} \quad n(0, t) = B^0/G_{hkl}(0, t) \tag{15}$$

$$\text{Regularity Condition:} \quad n(\infty, t)G_{hkl}(\infty, t) = 0 \tag{16}$$

$$\text{Initial Condition:} \quad n(h_{hkl}, 0) = n_0 \tag{17}$$

where ϕ_{hkl}^{kink} is the kink free energy (Winn and Doherty, 1998). The growth rate, G_{hkl}, is assumed to follow the screw dislocation growth mechanism. The secondary nucleation rate B^0 can be approximated by an empirical power law model, see Eq. 20 below.

Without loss of generality, the crystal shape factor $k_v(h_{hkl})$ in the above model is defined in the classic way (Randolph and Larson, 1988) as the ratio of crystal volume $V_{\text{cryst}}(h_{hkl})$ to the cube of the characteristic length h_{hkl}. For 2-D crystals, shape factors defined as in Eq. 10 can be used. The crystal shape factor will also change along with the size, as the crystal shape undergoes evolution during growth. As the crystals approaches their steady-state shape, the shape factor will reach a steady-state value, $k_{v,ss}$, which is analogous to the fixed shape factor used by other researchers.

It is worth noticing that the population balance model Eqs. 11 and 12 has a form identical to a conventional 1-D PBM (Randolph and Larson, 1988), except for the use of a size-dependent shape factor. For organic crystals grown from a single solvent, simple and effective methods have been recently developed to predict the steady-state morphology (Winn and Doherty, 1998) as well as the shape evolution (Gadewar and Doherty, 2004) which enables the computation of the shape factor for crystals of any size.

Numerical methods

The PBM model (11) is a hyperbolic partial-diffusion equation. Analytical solution of such a model is available under very limited conditions. In most cases, numerical solution has to be pursued instead. The objective of this research is not to develop a new numerical PBM solution method, but to use existing methods to show how crystals evolve their size and shape.

A large number of numerical methods have been proposed in the literature, some of which are discussed briefly here. Ramkrishna (2000) presented an excellent review of the numerical methods. They can be roughly classified into four categories: finite difference methods, method of weighted residuals, discretized population balance models, and Monte Carlo simulation methods. Finite difference methods are the simplest to formulate and are applicable to all types of problems. In these techniques, the number density derivatives are approximated by finite differences. The disadvantage of this method is the low accuracy and, consequently, the need for a large number of grid points. Spurious oscillations and numerical dispersions in the distributions are also reported, although the stability of the method is ensured for an adequate number of grid points. The weighted residual methods are most commonly used in the literature. In these techniques, the continuous number density function is expressed as a linear combination of a set of basis functions, and the weighted residuals of the PBM are driven to zero. Therefore, properly formulated weighted residual methods can generate a more accurate approximation of the crystal-size distribution than finite difference methods. However, these methods are more difficult to formulate and can be quite expensive in computational cost. The discretized population balance methods have emerged as a computationally efficient alternative from the late 1980's. They are essentially finite difference based methods formulated in the cumulative distribution function on finite intervals (bins), instead of the number density function on grid points. Consequently, they are inherently a coarser discretization scheme than the previous two classes of methods. In addition, these methods can not handle growth and nucleation accurately and efficiently. The Monte Carlo simulation methods are most suitable for stochastic complex systems with more than one spatial dimension, and can be rather computationally demanding.

On the basis of these considerations, we choose to use the finite difference method for the simulation of our population balance model. A finite size domain is chosen which is sufficiently large that almost all crystals in the crystallizer reside in this range (see the Discussion section for more details). A total number of 100 to 200 node points of h are used to ensure numerical stability. The actual number of node points is chosen according to the required numerical accuracy. The spatial derivatives are then approximated by finite differences, and the integrals are calculated using Simpson's formula. The discretized model is then

$$\frac{dn_i(t)}{dt} = -\frac{n_i(t)}{\tau} - G_{hkl}\frac{n_i(t) - n_{i-1}(t)}{\Delta h_{hkl}} \quad i = 1, \cdots, N \tag{18}$$

where n_0 is equal to $n(0, t)$, which is given by the boundary condition Eq. 15. The solute mass balance equation for the discretized PBM remains Eq. 12 in which ϵ is calculated as follows

$$\varepsilon = 1 - \sum_i^N s_i h_i^3 k_v(h_i) n_i$$

where h_i stands for the crystal size h_{hkl} at the i-th node point and s_i denotes the Simpson formula coefficients.

Case Study: Succinic Acid

Crystals of succinic acid grown from aqueous solution develop a plate-like shape, resembling a six-sided polygon at

Table 1. Succinic Acid Faces

Face	R_i	$\alpha_{i,i+1}$ (°)	v_i/G_{020}
0 (100)	0.239	—	—
1 (020)	1.000	$\alpha_{1,2} = 40.98$	0.936
2 (021)	1.062	$\alpha_{2,3} = 19.10$	−0.592
3 (011)	0.711	$\alpha_{3,4} = 29.92$	2.692
4 (002)	1.365	$\alpha_{4,5} = 29.92$	−1.893
5 ($0\bar{1}1$)	0.711	$\alpha_{5,6} = 19.10$	2.692
6 ($0\bar{2}1$)	1.062	$\alpha_{6,7} = 40.98$	−0.592
7 ($0\bar{2}0$)	1.000	$\alpha_{7,8} = 40.98$	0.936
8 ($0\bar{2}1$)	1.062	$\alpha_{8,9} = 19.10$	−0.592
9 ($0\bar{1}1$)	0.711	$\alpha_{9,10} = 29.92$	2.692
10 ($00\bar{2}$)	1.365	$\alpha_{10,11} = 29.92$	−1.893
11 ($01\bar{1}$)	0.711	$\alpha_{11,12} = 19.10$	2.692
12 ($02\bar{1}$)	1.062	$\alpha_{12,1} = 40.98$	−0.592

steady state, with a large dominant base plane (100). Therefore, it represents a good candidate 2-D crystal which can be handled with the current shape evolution model. The primary interest of this study is to investigate the shape evolution, and the relationship between the shape factor and crystal-size distribution.

Shape evolution

A detailed morphology investigation must be performed prior to the prediction of crystal shape evolution to reveal important information, such as the significant crystal faces that are likely to appear during the growth, the angles between the faces, and the relative normal growth rates of the faces. First principle methods, such as Liu et al. (1995) and Winn and Doherty (1998), are well suited for such investigation of solution-grown crystal morphologies, as these models explicitly account for the effect of solute-solvent interaction on the crystal morphology. Table 1 lists the likely growth faces for succinic acid grown from water, and their relative growth rates R_i, with respect to the (020) face, obtained from Winn and Doherty (2002). The angles between neighboring faces and the relative tangential velocities of each face, assuming all faces are present, are also listed in this table. The slowest growing dominant face is also listed in the table, although it is independent of the 2-D shape evolution.

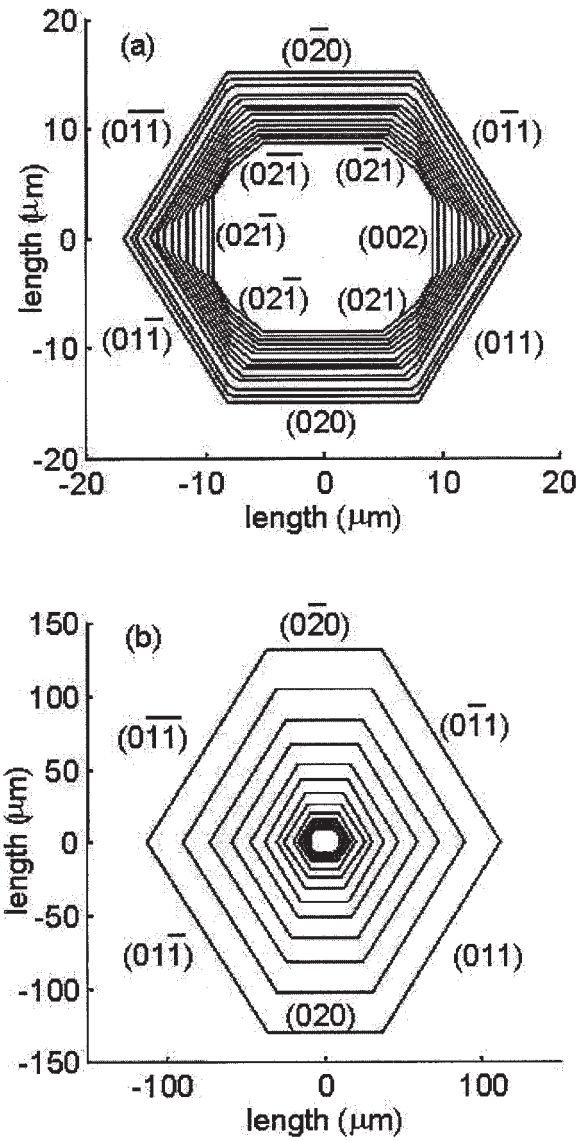

Figure 2. Shape evolution of a succinic acid crystal from a circle-like seed.

(a) Early stages; (b) later stages reaching steady state.

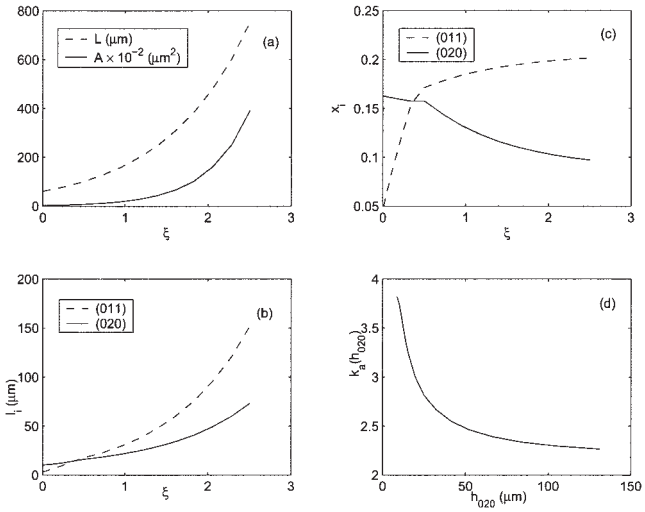

Figure 3. Evolution of succinic acid crystal physical variables.

(a) Perimeter (L) and area (A) vs. warped time ξ; (b) length of (011) and (020) face vs. warped time; (c) dimensionless length of (011) and (020) face vs. warped time; (d) area shape factor as a function of characteristic length, h_{020}.

Although the CSE model is capable of dealing with crystal seeds with arbitrary shapes, we start out study with some "well formed" seeds. First, a twelve-faced seed representing an approximate circle of radius $r = 10$ μm (all corner points are on this circle) is studied. The initial length of the (020) face is set to be $l^0_{020} = 10$ μm, and other quantities are calculated accordingly.

For this given seed, at a warped time $\xi_1 = 0.3473$, $L^{(1)}/L^0 = 1.4152$, faces (002) and (00$\bar{2}$) disappear. At the next transition time $\xi_2 = 0.5055$, $L^{(2)}/L^{(1)} = 1.1714$, faces (021), (0$\bar{2}$1), (02$\bar{1}$), and (02$\bar{1}$) disappear. After that, no faces disappear, and the crystal evolves toward its steady-state shape. Illustrative figures showing the evolution of size and shape of the crystals are shown in Figures 2a and 2b.

Several important quantities for the crystal shape and size evolution are plotted in Figure 3. The evolution of perimeter and area (since we are considering a 2-D crystal) of the crystal vs. the warped time, are shown in Figure 3a. Both are in the form of an exponential function, as predicted by Eq. 6 and Eq. 9. Figure 3b shows the change of the absolute length l_i, of faces (020) and (011) vs. the warped time. Figure 3c shows the ratio of the length of faces (020) and (011) to the total perimeter L, indicating that both x_{011} and x_{020} are converging to their steady-state values. Figure 3d shows the area shape factor vs. the perpendicular distance h_{020} of the chosen reference face. The shape factor function looks quite smooth, even during the transition times when face disappearance occurs. A simple

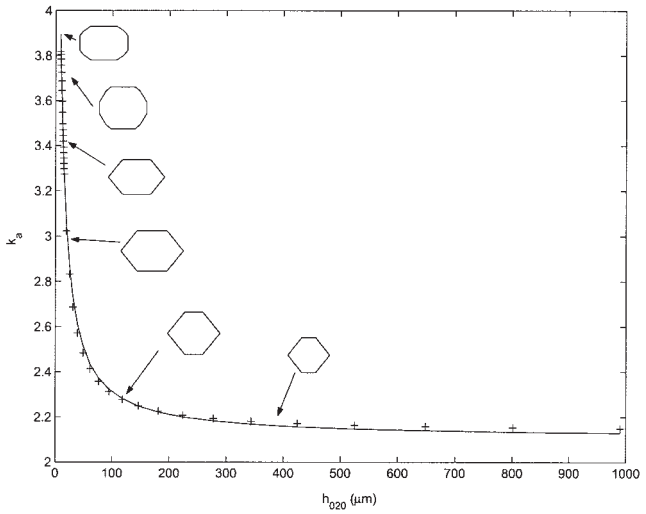

Figure 4. Shape factor: calculated points (+), curve fit (solid line).

second-order polynomial curve fit through the calculated points is shown in Figure 4. The fitted polynomial is as follows

$$k_a(h_{020}) = -0.469h_{020}^{-2} + 2.089h_{020}^{-1} + 2.131$$

The shape factor eventually converges to the constant value of 2.131 as the crystals grow into their steady-state shape. It is worth mentioning that the curve-fitting of the shape factor is not necessary. However, it provides a convenient way to obtain the shape factor at any given size.

The shape evolution of some non-circular-like seeds was also studied. The initial sizes and shapes of the seeds are listed in Table 2. The seeds are referred to as follows for convenience: (a) the 5-faced quasi square; (b) the asymmetric triangle; (c) the thin needle elongated in the [020] direction; (d) the thick needle elongated in the [002] direction. The four seeds have very different shapes, but all with an initial size of $h_{020}^0 = 10\ \mu$m. The early stages of shape evolution for these seeds are illustrated in Figure 5. During the early growth stages, the crystal shapes remain quite different from each other and all very far from the steady-state shape shown in Figure 2b, although they all eventually grow into the same steady-state habit.

Notice that these seeds have very different shapes, but all with the same initial characteristic length h_{020}^0. Therefore, they have quite different areas, and consequently different shape factor values. Simple calculation reveals that the area of the triangle seed ($k_a(h_{020}^0) = 2.1$) is about half of the 5-faced seed ($k_a(h_{020}^0) = 3.8$). The area of the thin needle ($k_a(h_{020}^0) = 0.4$) is only about 10% of the 5-faced seed, while the thick needle ($k_a(h_{020}^0) = 40.0$) is about 10 times as big as the 5-faced seed. It is of interest to investigate how fast these seeds evolve into their steady-state habit. The shape factors for crystals grown from these seeds are compared in Figure 6. The shape factors for the 12-faced seed and 5-faced seed are very close for all crystal sizes. For $h_{020} > 30\ \mu$m, although a crystal grown from the triangular seed may still have a quite different shape, its shape factor value is very close to that of the 12-faced and 5-faced seeds. On the other hand, when $h_{020} > 300\ \mu$m, the shapes as well as the shape factor values for crystals grown from these three seeds are almost identical.

In contrast, the shape factor evolution trajectories for the two needle-type seeds are quite different from the previous seeds. A crystal grown from the thin needle seed approaches steady-state shape quickly: for $h_{020} > 30\ \mu$m, it will have a shape very close to the steady-state habit, and for $h_{020} > 300\ \mu$m, its shape factor is also very close to the three seeds discussed earlier. Finally, it takes a crystal grown from the thick needle seed a long time to approach the steady-state shape. For all crystal sizes shown in the figure, its shape factor is much larger than crystals with the same characteristic length which are grown from other seeds. Computation also reveals (not illustrated in the figure) that this seed will not reach close ($k_a(h_{020}) = 2.20$) to its steady-state habit ($k_{a,ss}(h_{020}) = 2.13$) until $h_{020} > 5500\ \mu$m, while a crystal grown from the other seeds only needs to grow to 200 μm. These observations indicate that the speeds for crystals grown from different seed shapes to reach their steady-state shape can be very different (see Appendix A for a more detailed discussion), and, therefore, the shape factor for crystals with the same characteristic size can be very different. This provides some insights for engineering an appropriate seed shape for crystal growth. On the other hand, the difference in the shape factors for crystals grown from some different seed shapes may only be significant for very small sizes, and crystals with the same characteristic size, and the same volume may have quite different shapes. Therefore, we should bear in mind that the shape factor is a

Table 3. Growth and Nucleation Rate Parameters

Parameters	Value	Variables	Units in Power Law Models
k_B	1.70×10^6	B^0	1/(s · kg water)
b	2.42	c, c_s	kg/kg water
q	1.18	M_T	kg/kg water
j	0.543	G_{020}	μm/s
k_g	81.0	n_i	$(\text{liter})^{-1} \cdot \mu\text{m}^{-1}$
g	1.03		
ω	550 rpm		
c_s	104.29 g/(kg water)		

Table 2. Initial Size and Shape of the Noncircular Seeds, Length Unit is μm

Seed (a)			Seed (b)			Seed (c)			Seed (d)		
Faces	h_j^0	l_j^0	Faces	h_j^0	l_j^0	Faces	h_j^0	l_j^0	Faces	h_j^0	l_j^0
(020)	10.0	20.0	(020)	10.0	23.0	(020)	10.0	2.0	(020)	10.0	200.0
(00$\bar{2}$)	10.0	13.4	(00$\bar{2}$)	11.5	20.0	(00$\bar{2}$)	1.0	20.0	(00$\bar{2}$)	100.0	20.0
(0$\bar{2}$1)	9.2	10.0	(0$\bar{2}$1)	0.0	30.5	(0$\bar{2}$0)	10.0	2.0	(0$\bar{2}$0)	10.0	200.0
(0$\bar{2}$0)	10.0	12.5				(00$\bar{2}$)	1.0	20.0	(00$\bar{2}$)	100.0	20.0
(00$\bar{2}$)	10.0	20.0									

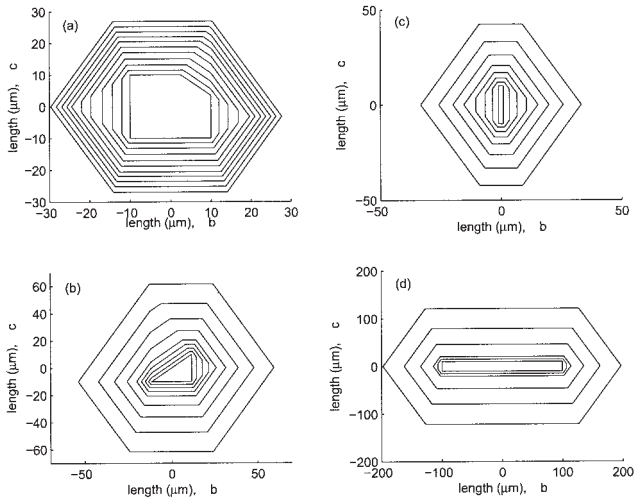

Figure 5. Shape evolution of succinic acid crystals from noncircle-like seeds.

(a) 5-faced seed; (b) triangular seed; (c) thin needle elongated in [020] direction; (d) thick needle elongated in [002] direction.

convenient measure to represent the crystal volume, but it does not suffice to describe the actual shape of a crystal.

CSD Dynamics

The steady state CSD for an ideal MSMPR crystallizer is in the form of an exponential function (Randolph and Larson, 1988), and when applied to our PBM gives

$$n_{ss}(h_{hkl}) = n_0 \exp(-h_{hkl}/\tau G_{hkl,ss}), \quad h_{hkl} \in (0, \infty)$$

In order to discretize the continuous PBM, we must truncate the infinite size domain at an upper limit, $h_{hkl,max}$, so that almost all crystals reside in the size range $(0, h_{hkl,max}]$. We can define the truncation error as

$$E_{tr} = 1 - \frac{m_0'}{m_0} = \exp(-h_{hkl,\max}/\tau G_{hkl,ss})$$

where m_0 is the zeroth moment of distribution at steady state ($m_0 = \int_0^\infty n(\infty, h_{hkl})dh_{hkl}$), and represents the total number of crystals of all sizes per unit volume, and m_0' stands for the number concentration of crystals in the size domain $(0, h_{hkl,\max}]$. For convenience, we choose $h_{hkl,\max}$ to be an integer number between $7\tau G_{hkl,ss}$ and $8\tau G_{hkl,ss}$ in this study, therefore, $E_{tr} < 0.1\%$. A good estimate of $G_{hkl,ss}$ is helpful in determining the size range. Trial and error was used to get the appropriate size domain.

In this study, the PBM was discretized using finite differences on a size domain of $h_{020} \in [10, 1500]$ μm, with $\Delta h = 10$ μm. The residence time and solute feed concentration are chosen as input variables, and $\tau = 0.5$ h, $c_{in} = 108$ g/kg water are used for the simulations. The crystallizer is assumed to be operated at 30°C. The saturation concentration and metastable zone width for succinic acid grown from water at this temperature are 104.29 g/kg water, and about 5 g/kg water, respectively (Qiu and Rasmuson, 1994). The face growth and secondary nucleation kinetics are assumed to follow empirical power law models

$$G_{020} = k_g \Delta c^g \tag{19}$$

$$B^0 = k_B \omega^q M_T^j \Delta c^b \tag{20}$$

The empirical growth model for the (020) face is obtained from Mullin and Whiting (1980), the secondary nucleation rate model is obtained from Qiu and Rasmuson (1994). The model parameters are listed in Table 3 for reference. It is worth noting that both of these models were estimated from batch cooling crystallization experiments. Although the kinetics for a continuous crystallizer may be different, we assumed these parameters were also valid for continuous crystallizers.

The solubility and solute concentrations used in Eqs. 19 and 20 (cf. Table 3) are based on solvent mass (kg solute/kg solvent), while these variables in our PBM Eq. 12 are based on clear solution volume (kg solute/liter liquid phase volume). The conversion between these two forms of solute concentration requires knowledge of the density of the supersaturated solution. As supersaturation for succinic acid is comparatively low, we use the density of a saturated solution as an approximation, From the correlation of Findlay (1955), the density of saturated aqueous solution of succinic acid at 30°C is $\rho_{\text{sat}} = 1.0246$ kg/liter. The conversion of concentration is then

$$c_{\text{liq}} = \rho_{\text{sat}} \frac{c_{\text{sol}}}{1 + c_{\text{sol}}}$$

where c_{liq} and c_{sol} stand for solute concentrations, based on clear liquid phase volume, and per kilogram of solvent, respectively.

The simulation results for the 12-faced seed are shown in the Figures 7–9. The initial CSD is chosen to be a linear distribution in the size range [10, 500 μm]. Figure 7 shows the temporal changes of the important variables. The crystallizer reaches steady state in about 4–6 h. The initial and final CSDs are shown in Figure 8. As expected, the steady-state CSD has

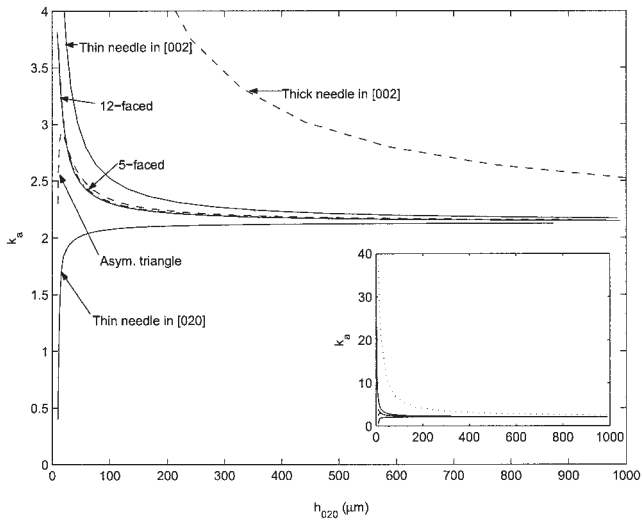

Figure 6. Effect of seed shape on the shape factor.

Table 4. Measured Relative Growth Rates of Individual Faces for Succinic Acid Grown from Water (Mullin and Whiting, 1980). [Δc] = kg/kg Water

Crystal Faces	Growth Correlation (μm/s)	$R_{(1)}$	$R_{(2)}$	$R_{(3)}$	$R_{W\&D}$
(020)	$81.0 \times \Delta c^{1.03}$	1.0	1.0	1.0	1.0
(011)	$145.0 \times \Delta c^{1.15}$	0.781	0.827	0.951	0.711
(100)	$270 \times \Delta c^{1.48}$	0.149	0.184	0.308	0.239

the shape of a exponential function. The crystal shapes at certain sizes are also illustrated along with the CSD in Figure 8. Figure 9 shows the temporal evolution of the crystal number density function over the size intervals.

For comparison, simulations were performed for seeds of other shapes as shown in Figure 5, with seed size (h^0_{020}), initial CSD, and all other physical properties and operating parameters the same as in the previous simulation. The temporal evolution of the important process variables, as well as the steady-state CSD for the 5-faced and triangular seeds are indistinguishable from those of the twelve-faced seed. The results for the thin needle elongated in [020] direction are also virtually identical to those of the twelve-faced seed. The steady-state CSD for a triangular seed is shown in Figure 10 as an example. Under these operating conditions, the mass fraction of crystals of size less than 30 μm (which accounts for about 10% of the total number of crystals), where the shape factors are significantly different, is only about 0.01% of the total solid-phase mass. Therefore, the impact of shape differences in small crystals on the solute mass balance (and, therefore, the supersaturation) is numerically negligible. Consequently, the temporal evolutions, as well as steady-state solutions of the PBM for these seeds are numerically the same. In fact, the mass fraction of crystals in a much larger range, from 10 to 200 μm, which accounts for about 63% of the total number of crystals, is still only 2% of the total solid phase mass. Therefore, for the above seed shapes, even using the fixed steady-state shape factor for crystals of all sizes will still render virtually the same results.

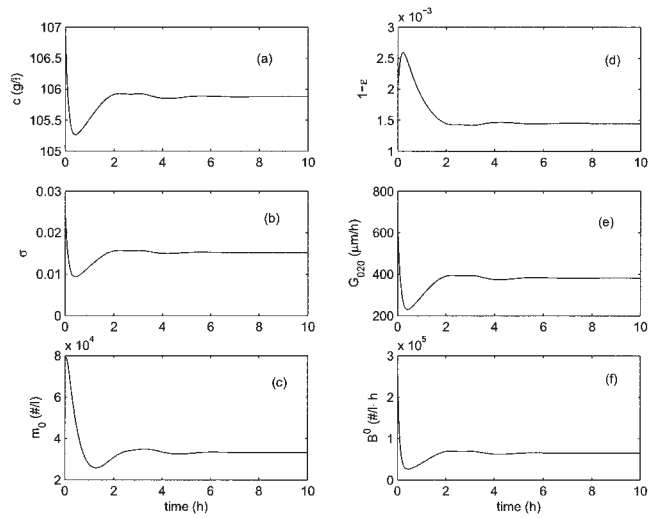

Figure 7. Crystallizer process variables, τ = 0.5 h, c_{in} = 108 g/kg water.

(a) Solute concentration; (b) relative supersaturation; (c) total number concentration of crystals; (d) solid phase volume fraction; (e) growth rate; (f) nucleation rate.

In contrast, the temporal evolutions and steady-state CSD for the thick needle are quite different from those of the other seeds, as shown in Figures 11 and 12. This is due to the fact that crystals grown from this type of seed grow into their steady-state shape very slowly (see Figure 6). Under the operating conditions investigated, all crystals in the given size range [10, 1500] μm are quite different from their steady-state habit, and the shape factors are significantly larger than the steady-state value.

Discussion

As mentioned earlier in the second section of this paper, the relative face growth rate of all major crystallographic faces is required for the shape evolution model. In this study, the relative growth rates are calculated using the predictive method of Winn and Doherty (1998). A key assumption of this method is that the face growth rate is controlled by kink-integration and, therefore, the relative growth rates of all faces are constant, independent of supersaturation and crystal size. Under real crystal growth situations, when the bulk and/or surface diffusion effects are not negligible, the relative growth rates may vary with supersaturation. For instance, Mullin and Whiting (1980) have measured the growth of the major faces for succinic acid crystals grown from aqueous solution. Power law correlations with different power dependence on the supersaturation were reported for these face growth rates, as listed in Table 4. Table 4 also lists the calculated relative growth rates for three different supersaturations of Δc_1 = 1 g/kg, Δc_2 = 1.6 g/kg, and Δc_3 = 5 g/kg, respectively, using Mullin and Whiting's correlations. The supersaturations Δc_1 and Δc_3 represent the approximate lower and upper bounds of the meta-

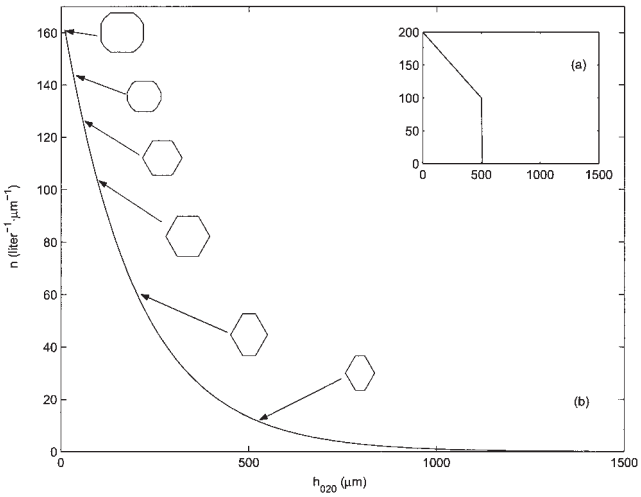

Figure 8. Crystal-size distribution and shape distribution, β = 0.5 h, c_{in} = 108 g/kg water.

(a) Initial and (b) steady-state distributions.

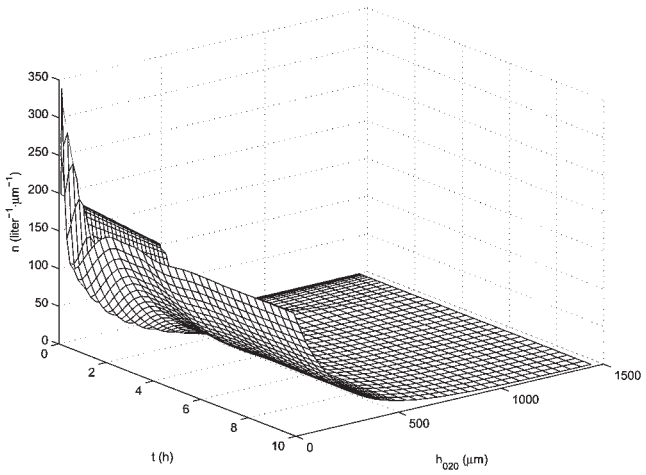

Figure 9. Evolution of crystal-size distribution, τ = 0.5 h, c_{in} = 108 g/kg water.

stable zone, and Δc_2 corresponds to the steady-state supersaturation in the previous case study for the twelve-faced seeds. The relative growth rates predicted by Winn and Doherty ($R_{W\&D}$) are also listed for comparison.

From the table, we see that Mullin and Whiting's correlation gives larger relative growth rates for the (011) face than Winn and Doherty's method. Consequently, the steady-state crystal habit predicted with Winn and Doherty's model is slightly "elongated" along the [020] direction, as shown in Figure 13. Overall, the crystal shape predicted by Winn and Doherty is in good agreement with those from Mullin and Whiting's experimentally measured correlation.

From these results, we can see that under normal operating conditions where supersaturation is low, the fixed relative face growth rates assumption represents a good approximation to the real situation even during the transient period where Δc is not constant. Moreover, when the crystallizer is being operated at steady state, the supersaturation is constant, and the relative growth rates are constant even when the face growth rates have different dependencies on Δc. Therefore, the method developed in this article is expected to give satisfactory results for size and shape evolution in both these cases.

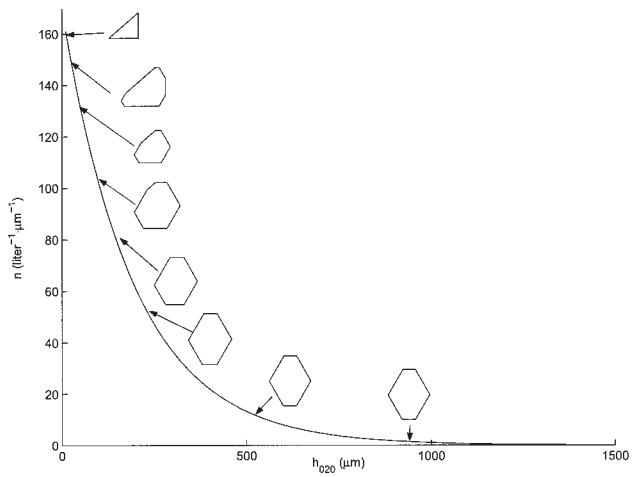

Figure 10. Steady-state crystal size and shape distribution for triangular seeds, τ = 0.5 h, c_{in} = 108 g/kg water.

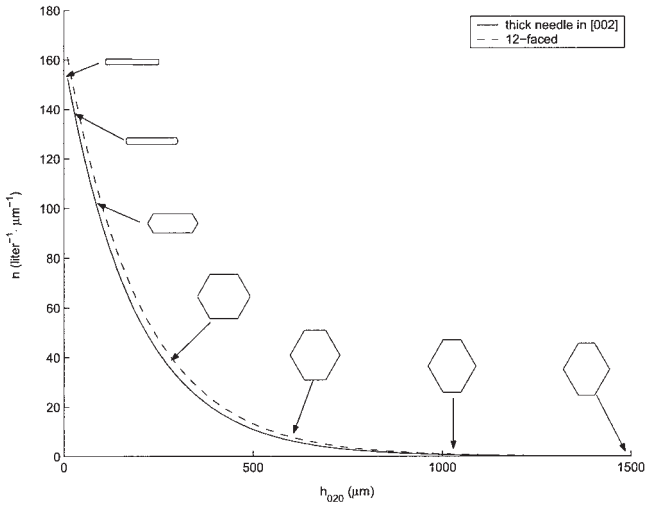

Figure 11. Steady-state crystal size and shape distribution for the thick needle, τ = 0.5 h, c_{in} = 108 g/kg water.

For the transient period with higher supersaturation when the diffusion effects are significant, faces may grow with a significantly different dependence on supersaturation, hence, the relative face growth rates change with time. The shape of a crystal is then dependent on its current size, the seed size and shape, and the supersaturation history profile where it was grown. That is to say, crystals of a certain characteristic size grown from seeds of the same size and shape may have a different habit. Therefore, the crystal shape can not be represented by a single shape factor, which depends only on the size. Consequently, a multidimensional PBM is required to describe the simultaneous evolution in crystal shape and size.

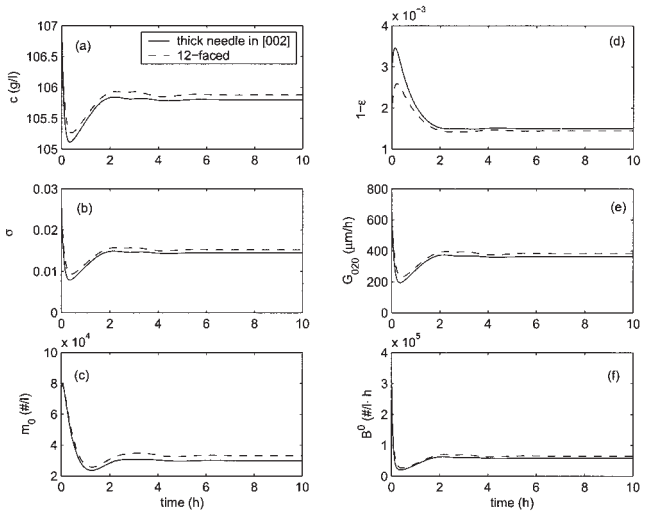

Figure 12. Crystallizer process variables for the thick needle, τ = 0.5 h, c_{in} = 108 g/kg water.

(a) Solute concentration; (b) relative supersaturation; (c) total number concentration of crystals; (d) solid phase volume fraction; (e) growth rate; (f) nucleation rate.

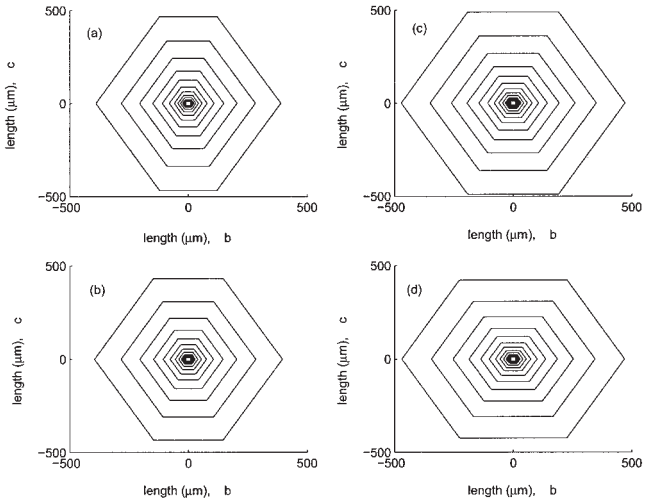

Figure 13. Comparison of crystal habit using different face growth kinetic models.

(a) Constant relative growth rates (Winn and Doherty, 1998); (b)–(d) supersaturation-dependent relative growth rates (Mullin and Whiting, 1980), (b) $\Delta c = 1.0$ g/kg water; (c) $\Delta c = 1.6$ g/kg water; (d) $\Delta c = 5.0$ g/kg water.

Summary

We have developed a method to simultaneously predict crystal shape evolution and size distribution, by combining shape evolution and population balance models. With the assumption that all significant crystal faces grow with the same kinetic mechanism, we are able to use a piecewise smooth shape factor dependent only on the crystal size to describe the crystal volume and, therefore, link the shape evolution to a 1-D population balance model. The influence of initial seed shape on the shape evolution, and CSD dynamics are also investigated. The influence of supersaturation dependent face growth rates on the steady-state crystal habit, and the possible extension of the current method are also discussed.

Acknowledgments

Financial support from Rhodia, Inc. is gratefully acknowledged.

Notation

A_{cryst} = area of the dominant crystal face, μm^2
B^0 = nucleation rate, 1/(s · kg solvent)
b, g = order for power law models, for growth and nucleation rates
c = solute concentration in the crystallizer, kg/kg solvent
c_{in} = solute concentration in the feed stream, kg/kg solvent
c_s = solubility, kg/kg solvent
Δc = supersaturation, kg/kg solvent
E_{tr} = truncation error
G = overall crystal growth rate, μm/s
G_d = normal growth rate of the dominant face, μm/s
G_i = normal growth rate of face i, μm/s
G_{hkl} = normal growth rate of the reference face, μm/s
(hkl) = Miller index of the crystallographic face
h_d = normal distance of the dominant face, μm
h_d^0 = initial normal distance of the dominant face, μm
h_i = normal distance of face i, μm
h_i^0 = initial normal distance of face i, μm
h_{hkl} = normal distance of the reference face, μm
$h_{hkl,\max}$ = upper limit of the truncated size domain, μm
Δh = discretization step size, μm
k_a = area shape factor
k_g, k_B = coefficients for power law model
k_i = BCF growth model coefficients
k_v = volume shape factor
l_i = length of face i, μm
L = perimeter of the dominant crystal face, μm
L^0 = initial perimeter of the dominant crystal face, μm
m_0 = total crystal number concentration, 1/L
m_0' = total crystal number concentration in finite size domain, 1/L
M = total number of crystal faces
N = total number of discretization node points
n = crystal number density function, 1/L · μm
n_i = crystal number density function at i-th node point, 1/L · μm
r = radius, μm
R_d = relative growth rate of the dominant face
R_i = relative growth rate of face i
R_{ij} = ratio of growth rates for face i and j
u_i = dimensionless tangential growth rate for face i
v_i = tangential growth rate of face i, μm/s
V = summed tangential growth rate, μm/s
V_{cryst}, V_i = crystal volume, μm^3
x_i = fraction of length for face i
y_i = dimensionless tangential growth rate of face i
Y = summed dimensionless tangential growth rate

Greek letters

$\alpha_{i,j}$ = angle between face i and j
α_i, β_i, γ_i, ζ_i = coefficients of the polynomial for the volume shape factor as a function of the characteristic length
ϵ = volume fraction of liquid phase in crystallizer
ω = impeller speed, rpm
ϕ_i^{kink} = kink free energy of face i, kJ/mol
ρ = density of crystalline material, kg/m^3
σ = relative supersaturation
$\sigma_{1,i}$ = strength of dislocation source i
τ = residence time, h
ξ = warped time

Subscripts and superscripts

0 = initial
i = face i
in = feedstream
d = dominant face
hkl = reference face
ss = steady-state
sol = based on per kilogram solvent
liq = based on per liter clear liquid phase volume
$W\ \&\ D$ = Winn and Doherty's method, 1998

Literature Cited

Benallou, A., D. E. Seborg, and D. A. Mellichamp, "Dynamic Compartmental Models for Separation Processes," *AIChE J.,* **32**, 1067 (1986).

Bermingham, S. K., H. J. M. Kramer, and G. M. van Rosmalen, "Towards On-Scale Crystallizer Design Using Compartmental Models," *Comp. Chem. Eng.,* **22**, 355 (1998).

Bisker-Leib, V., and M. F. Doherty, "Modeling Crystal Shape of Polar Organic Materials: Applications to Amino Acids," *Crystal Growth and Design,* **3**, 221 (2003).

Burton, W. K., N. Cabrera, and F. C. Frank, "The Growth of Crystals and the Equilibrium Structure of Their Surfaces," *Philos. Trans. Roy. Soc.,* **243**, 299 (1951).

Findlay, A., *Practical Physical Chemistry,* 8th ed., Longmans, London, UK (1955).

Gadewar, S. B., and M. F. Doherty, "A Dynamic Model for Evolution of Crystal Shape," *J. Crystal Growth*, 267, 239 (2004).

Hulbert, H. M., and S. Katz, "Some Problems in Particle Technology. A Statistical Mechanical Formulation," *Chem. Eng. Sci.,* **19**, 555 (1964).

Jetten, L. A. M. J., H. J. Hunan, P. Bennema, and J. P. van der Erden, "On the Observation of the Roughening Transition of Organic Crystals Growing from Solution," *J. Crystal Growth,* **68**, 503 (1984).

Kozlovskii, M. I., "Kinetics of Crystallization at Constant Temperature and Supersaturation," *Kristallografiya,* **2**, 760 (1957).

Kramer, H. J. M., J. W. Dijkstra, A. M. Neumann, R. O. Meadhra, and G. M. van Rosmalen, "Modelling of Industrial Crystallizers, A Compartmental Approach Using a Dynamic Flow-Sheeting Tool," *J. Crystal Growth,* **166**, 1084 (1996).
Liu, X. Y., E. S. Boek, W. J. Briels, and P. Bennema, "Prediction of Crystal Growth Morphology Based on Structural Analysis of the Solid-Fluid Interface," *Nature,* **374**, 342 (1995).
Ma, D. L., D. K. Tafti, and R. D. Braatz, "Optimal Control and Simulation of Multidimensional Crystallization Processes," *Comp. Chem. Eng.,* **26**, 1103 (2002).
Mullin, J. W., and M. J. L. Whiting, "Succinic Acid Crystal Growth Rates in Aqueous Solution," *Ind. Eng. Chem. Fundam.,* **19**, 117 (1980).
Prywer, J., "Three-Dimensional Model of Any Shape Face Disappearance in Crystal Habit," *J. Cryst. Growth,* **158**, 568 (1996).
Qiu, Y., and A. C. Rasmuson, "Estimation of Crystallization Kinetics from Batch Cooling Experiments," *AIChE J.,* **40**, 799 (1994).
Ramkrishna, D., *Population Balances: Theory and Applications to Particulate Systems in Engineering,* Academic Press, San Diego, CA (2000).
Randolph, A. D., and M. A. Larson, *Theory of Particulate Processes: Analysis and Techniques of Continuous Crystallization,* Academic Press, New York, NY (1988).
Singh, N. B., T. Henningsen, E. P. A. Metz, R. Hamacher, E. Cumberledge, R. H. Hopkins, and R. Mazelsky, "Solution Growth of Vanillin Single Crystals," *Materials Letters,* **12**, 270 (1991).
Szurgot, M., and J. Prywer, "Growth Velocities and Disappearance of Faces of Crystals," *Cryst. Res. Tech.,* **26**, 147 (1991).
Winn, D., and M. F. Doherty, "A New Technique for Predicting the Shape of Solution-Grown Organic Crystals," *AIChE J.,* **44**, 2501 (1998).
Winn, D., and M. F. Doherty, "Modeling Crystal Shapes of Organic Materials Grown from Solution," *AIChE J.,* **46**, 1348 (2000).
Winn, D., and M. F. Doherty, "Predicting the Shape of Organic Crystals Grown from Polar Solvents," *Chem. Eng. Sci.,* **57**, 1805 (2002).

Appendix

(A) Transition to steady-state habit

From the CSE model, it is clear that a crystal grown from an arbitrary initial shape will never reach its steady-state habit until infinite time. Practically, however, crystals approach their steady state fairly quickly. Various index quantities can be defined as an indicator of how close a crystal is to its steady-state shape. In this article, the area/volume shape factor has been used for this purpose. Another commonly used index is the ratio of normal distances from an internal origin to the major crystal faces. Using the Wulff-Chernov steady-state condition, the ratio of the normal distances of any two faces, h_i and h_j is equal to the ratio of their relative normal growth rates, R_i and R_j, that is

$$\left(\frac{h_i}{h_j}\right)_{ss} = \frac{R_i}{R_j} = K \tag{A1}$$

where K is a known constant. From Eq. 8, we also have the following relation for all time t

$$\frac{h_i(t) - h_i^0}{h_j(t) - h_j^0} = K$$

We define that at a certain time θ, the crystal will reach a preset "satisfactory" criterion as having approximately steady-state habit, that is

$$\frac{h_i(\theta)}{h_j(\theta)} = K_1 \cong K$$

Also define the initial ratio as $h_i^0/h_j^0 = \alpha$, then we have

$$h_i(\theta) - h_i^0 = K(h_j(\theta) - h_j^0)$$

$$K_1 h_j(\theta) - \alpha h_j^0 = K h_j(\theta) - K h_j^0$$

$$\frac{h_j(\theta)}{h_j^0} = \frac{K - \alpha}{K - K_1}, \quad \frac{h_i(\theta)}{h_i^0} = \frac{K_1(K - \alpha)}{\alpha(K - K_1)} \tag{A2}$$

A simple example illustrates how long it will take to reach the steady state. Assume $K = 1.50$, $K_1 = 1.45$, and an initial seed of $\alpha = 1.0$, then the crystal need only grow 10 times larger in the h_j direction, and 14.5 times larger in the h_i direction to reach close to the steady-state habit. In contrast, if the initial seed has a needle-like shape with $\alpha = 0.1$, then the crystal must grow 28 times larger in the h_j direction and 406 times larger in the h_i direction to be considered at its steady-state shape. This dramatic increase is in accordance with common sense that crystal seeds with "far from steady-state shape" take longer to grow into their steady-state habit.

(B) Smoothness of the shape factors

From the CSE model solutions, we have the following expression for the area shape factor k_a in terms of the independent variable h_{hkl}

$$k_a(h_{hkl}) = \sum_i \left[\alpha_i + \beta_i(h_{hkl} - h_{hkl}^0)^{-1} + \gamma_i(h_{hkl} - h_{hkl}^0)^{-2}\right]$$

where

$$\alpha_i = u_i R_i Y, \quad \beta_i = u_i h_i^0 Y + R_i x_i^0 L^0, \quad \gamma_i = x_i^0 h_i^0 L^0$$

During any growth period when no face appears or disappears, all these parameters are constant, therefore, the shape factor is smooth in h_{hkl}. At any transition moment $\xi = \xi_t$, we need to compare $dk_a/dh_{hkl}|_{\xi_t^-}$ against $dk_a/dh_{hkl}|_{\xi_t^+}$ to determine the smoothness. We have

$$\frac{dk_a}{dh_{hkl}} = \frac{1}{2h_{hkl}^2}\sum_i \left(h_i \frac{dl_i}{dh_{hkl}} + l_i \frac{dh_i}{dh_{hkl}}\right) - \frac{1}{h_{hkl}^3}\sum_i l_i h_i$$

$$= \frac{1}{2h_{hkl}^2}\sum_i y_i h_i + \frac{1}{2h_{hkl}^2}\sum_i l_i R_i - \frac{1}{h_{hkl}^3}\sum_i l_i h_i \tag{A3}$$

In the above expression, the relative growth rates R_i, are always constant, and the face lengths and normal distances changes continuously: $h_i(\xi_t^-) = h_i(\xi_t^+)$, $l_i(\xi_t^-) = l_i(\xi_t^+)$. Therefore, the second and third terms in the above expression do not change during transitions (for appearing or disappearing faces j we have $l_j(\xi_t^-) = l_j(\xi_t^+) = 0$). However, y_i does change during transition, because the neighboring faces change (see Eq. 4), and the value of first term on the RHS of Eq. A3 is normally not the same before and after the transition. Therefore, $dk_a/dh_{hkl}|_{\xi_t^-} \neq dk_a/dh_{hkl}|_{\xi_t^+}$, that is, the area shape factor is only piecewise smooth.

Manuscript received July 28, 2003, and revision received Dec. 16, 2003.